CrystEngComm

Growth and characterization of ternary $BiScO_3$-$Pb(Cd_{1/3}Nb_{2/3})O_3$-$PbTiO_3$ ferroelectric single crystals with high Curie temperature

Journal:	*CrystEngComm*
Manuscript ID	CE-ART-03-2020-000473.R1
Article Type:	Paper
Date Submitted by the Author:	22-May-2020
Complete List of Authors:	Luo, Zeng; Xi'an Jiaotong University Zhuang, Jian; Xi'an Jiaotong University, Liu, Zenghui; Xi'an Jiaotong University, ; Simon Fraser University , Department of Chemistry Zhang, Nan; Xi'an Jiaotong University, a. Electronic Materials Research Laboratory, Key Laboratory of the Ministry of Education & International Center for Dielectric Research Ren, Wei; Xi'an Jiaotong University, Ye, Zuo-Guang; Simon Fraser University, Chemistry

Growth and characterization of ternary $BiScO_3$-$Pb(Cd_{1/3}Nb_{2/3})O_3$-$PbTiO_3$ ferroelectric single crystals with high Curie temperature

Zeng Luo[1], Jian Zhuang[1], Zenghui Liu[1,2], Nan Zhang[1,*], Wei Ren[1], and Zuo-Guang Ye[2,*]

[1] Electronic Materials Research Laboratory, Key Laboratory of the Ministry of Education & International Center for Dielectric Research, Faculty of Electronic and Information Engineering, Xi'an Jiaotong University, Xi'an 710049, China

[2] Department of Chemistry and 4D LABS, Simon Fraser University, Burnaby, British Columbia, V5A 1S6, Canada

*Email addresses: zye@sfu.ca and nzhang1@xjtu.edu.cn

Abstract

Ferroelectric single crystals of the ternary perovskite solid solution, $BiScO_3$-$Pb(Cd_{1/3}Nb_{2/3})O_3$-$PbTiO_3$ (BS-PCN-PT), has been successfully grown by the top-seeded solution growth method for the first time. The crystals with dimensions up to 2.5×2.5×1 cm^3 were obtained. The structure of the BS-PCN-PT crystals has been studied by high-resolution X-ray diffraction, combined with Polarized Light Microscopy, showing a tetragonal symmetry. The grown crystals exhibit a pseudo-cubic morphology with (001) facets, suggesting a dominant {100}-growth process. Interestingly, a single ferroelastic domain state was found in most (001) platelets cut from the as-grown crystal and carefully investigated by a combination of Polarized

Light Microscopy and Piezoresponse Force Microscopy. The single-domain crystals possess a high average coercive field (E_c ~ 30 kV/cm) and a high remanent polarization (25 μC/cm^2). An unpoled piezoelectric constant d_{33} of single-domain crystal is up to 111 pC/N due to its self-polarization. The Curie temperature T_C is found to be 423 ^{o}C by means of dielectric measurements, which is much higher than the relaxor-based $Pb(Mg_{1/3}Nb_{2/3})O_3$-$PbTiO_3$ (PMN-PT) piezocrystals. Moreover, the dielectric properties exhibit an excellent thermal stability up to 300 ^{o}C. A careful discussion about how domain state may affect electromechanical properties has been carried out. The high T_C, large coercive electric field, and high remanent polarization of the single-domain BS-PCN-PT crystals make this material a promising candidate for applications in a wider temperature range and at higher power than the PMN-PT crystals.

Keywords: Crystal structure, High resolution X-ray diffraction, Polarized light microscopy, Domain structure, Top seeded solution growth, Ferroelectric materials

Introduction

The well-known ferro-/piezoelectric materials like $Pb(Mg_{1/3}Nb_{2/3})_3$-$PbTiO_3$ (PMN-PT), and $Pb(Zn_{1/3}Nb_{2/3})O_3$-$PbTiO_3$ (PZN-PT) with complex perovskite structures are promising candidates for practical applications such as sensors, transducers, actuators and other devices, however, their low Curie temperatures and low coercive filed usually prohibit their applications at high temperatures.[1-4] Therefore, it is necessary to develop high-temperature and high coercive field ferro-/piezoelectric materials to meet the increasing demand for devices capable of operating at severe environments. As one of the promising materials, $BiScO_3$-$x$$PbTiO_3$ (BS-PT) ceramics were first shown to exhibit

a better piezoelectric response and a higher Curie temperature (T_C = 450 °C, d_{33} = 460 pC/N) with the MPB compositions, than the traditional materials based on $PbZrO_3$-$PbTiO_3$ (PZT).[5, 6] Several studies were performed on the BS-PT binary systems, revealing its excellent ferroelectric and piezoelectric properties.[7-14] However, this system has the drawback of high cost of scandium oxide, making it less attractive to industrial applications. To solve this problem, chemical substitutions and introduction of a third component into the BS-PT binary system have been carried out.[15-17] Among those new systems, (0.95-x)$BiScO_3$-0.05$Pb(Cd_{1/3}Nb_{2/3})O_3$-$x$$PbTiO_3$ (BS-PCN-xPT) polycrystalline ceramics were reported to exhibit good electric properties (T_C = 403 °C, d_{33} = 505 pC/N) with composition near the MPB region (x = 0.60).[18]

In our previous studies, the BS-PCN-xPT single crystals with compositions around the MPB were successfully grown by the top-cooled solution growth (TCSG) method, which exhibit a crossover from the rhombohedral to tetragonal phase.[19] In addition, they have a high Curie temperature of 450 °C and a large coercive field (E_C = 40 kV/cm), showing decent ferroelectric properties for high temperature and high-power applications.[19] Despite the progress made in the growth of the novel complex perovskite BS-PCN-xPT crystals, some major issues remain to be solved. Compositional variations occurred because the crystallization took place both on the surface of molten flux and around the crucible walls due to the lack of effective nucleation spots. Moreover, only tiny crystals are typically obtained by the TCSG method, which are too small for industrial applications that require high composition uniformity and large size. To meet the various demands in practical applications, it is essential to develop

effective techniques to grow large and high-quality crystals and systematically characterize their properties. The top-seeded solution growth (TSSG) method is an effective way to grow large and high-quality crystals, because its unique crystallization process and its slow growth under a specially designed temperature field can lead to high compositional homogeneity and controlled morphology. It has been wildly used for growing lead-based single crystals, such as PMN-PT[20, 21], PZN-PT[22], $Pb(Y_{1/2}Nb_{1/2})O_3$-$Pb(Mg_{1/3}Nb_{2/3})O_3$-$PbTiO_3$[23, 24], $Bi(Zn_{1/2}Ti_{1/2})O_3$-$PbZrO_3$-$PbTiO_3$[25], etc. However, it has not been used to grow the BS-PT based crystals. In the present work, we have grown the large single crystals of BS-PCN-PT by the TSSG method and investigated their crystal structure, domain structure, phase transitions, and electric properties.

Experimental

The top-seeded solution growth method was used to grow the single crystals of a nominal composition $0.35BiScO_3$-$0.05Pb(Cd_{1/3}Nb_{2/3})O_3$-$0.60PbTiO_3$ (BS-PCN-PT). The starting materials of high purity, PbO (99.9%), Bi_2O_3 (99.9%), TiO_2 (98%), Sc_2O_3 (99.99%), CdO (99%), and Nb_2O_5 (99.5%), were weighed according to the stoichiometry amounts of the given composition. Then they were mixed with the flux of composition (60 wt% PbO + 40 wt% Bi_2O_3) according to an optimized flux : solute weight ratio of 6 : 1. The mixture was homogeneously ground for 0.5 h before being loaded into a 50ml Pt crucible. The loaded Pt crucible was then put into a larger alumina crucible. At last, the alumina crucible was placed inside a single crystal growth furnace with a platinum rod hanged on the top of the furnace. The furnace and crucible set up

are shown in Fig. 1(a). The TSSG was achieved by a small seed crystal obtained from the BS-PCN-PT crystals previously grown by the top-cooled solution growth method.[19] The seed crystal was tied to the end of an alumina rod by platinum wire. Figure 1(b) gives a typical thermal profile used in the growth process, which consists of the following steps: the solution was heated from room temperature to T_1 = 1150 ^oC at a rate of R_1 = 275 $^oC/h$, followed by a dwelling of t_d = 12 h. Then the solution was cooled to T_2 = 980 ^oC in 3 days. T_2 was the saturation growth temperature determined experimentally, at which the seed crystal was introduced into the solution. The position of the seed crystal was about 2 mm below the surface of the melt. During the growth process, the cooling rate R_2 was about 5 ^oC/day. Upon cooling to T_3 = 953 ^oC, crystallization around the seed crystal started to take place. At the end of the growth (T_4 = 900 ^oC), the grown crystal was pulled slightly out of the melt, followed by a relatively fast cooling from 900 ^oC to room temperature in 12 h. The residual flux on the surface of crystals was cleaned by leaching in dilute hot HNO_3 solution.

The composition of the grown crystals was analyzed by energy dispersive X-ray spectroscopy (EDX) on a scanning electron microscope (FEI, Quanta FEG). The crystal structures of the as-grown crystals were determined on fine crushed powder by utilizing a PANalytical X'Pert Pro MPD diffractometer (40 mA, 40 kV, step size = 0.02 ^{o}/step, $2\theta = 20^o - 100^o$). In order to confirm the orientation of the as-grown crystals, X-ray diffraction analysis was carried out on the naturally grown facets of the crystals on a PANalytical Empyrean diffractometer (40 mA, 45 kV, step size = 0.02 ^{o}/step, $2\theta = 20^o - 90^o$).

The domain structures of the BS-PCN-PT crystals were examined by means of Polarized Light Microscopy (PLM) and Piezoresponse Force Microscopy (PFM). The as-grown crystals were cut parallel to the $(001)_{cub}$ plane to prepare the $(001)_{cub}$ platelets which were then carefully polished using a sand paper (1000/1200 grit) and a series of aluminium lapping films (5 to 1 μm, 3M) consequently, while leaving one of the naturally grown facets untouched as reference. The PLM experiments were performed using an Olympus BX-51 polarizing microscope equipped with an Olympus DP27 digital camera. The extinction behavior was analyzed by rotating the crystal position between the crossed analyzer and polarizer. The orientation of the optical indicatrix sections of the crystals was determined with the help of an Olympus U-CTB compensator at the wavelength of 546.1 nm. The crystal for PFM measurement was mounted on a piece of silicon with silver paste. A modified commercial atomic force microscopic system (AFM, Dimension ICON, NanoScope V, Bruker) was used in piezoresponse mode for imaging the ferroelectric domain structure at room temperature. The samples were annealed in air at 550 °C for 1 h to release the stress arising from the polishing process before any domain characterizations and analyses.

For electrical characterization, the polished $(001)_{cub}$-oriented BS-PCN-PT crystal platelets were painted with silver paste and gold wires were attached to both sides of the samples as electrodes. The ferroelectric hysteresis loops were displaced on the $(001)_{cub}$ platelets at room temperature by means of a Radiant RT-66 standardized ferroelectric testing system. Crystals for piezoelectric measurements were poled in a silicon oil bath under a field of 67.5 kV/cm at 120 ^{o}C for 15 min. Before and after poling,

a piezoelectric d_{33} meter (ZJ-6B, Institute of Acoustics Chinese Academy of Science) was used to measure the piezoelectric coefficient. The dielectric constant and loss tangent of the crystals were measured as a function of temperatures from room temperature (RT) to 500 ^{o}C at the frequency of 500 kHz using a 4980 Precision LCR meter (Agilent, Hewlett-Packard, USA) and a home-made temperature chamber. The heating rate was controlled by a temperature controller (EUROTHERM 3204 PID).

Results and discussion

Crystal growth

Figures 2(a) and (b) show the BS-PCN-PT single crystals grown by the TSSG method. A yellow crystal of large size (up to 2.5×2.5×1 cm^3) was obtained, and it exhibits a fully developed cubic shape with clear edges which can be seen from both top Fig. 2(a) and bottom Fig. 2(b) views. Compared with the TCSG method used in our previous work[19] by which only small crystals (of around 2-3 mm size) were obtained, the size and quality of the BS-PCN-PT crystals were significantly improved when grown by the TSSG method. It is believed that the specially designed temperature profile and the appropriate slow cooling rate provided a favorable convection process in the solution to promote the seeded growth. When the temperature was cooled down to the saturation-growth temperature at which the super-saturation was first reached, the seed crystal was introduced into the solution and it started to trigger a stable nucleation around it. As an effective supper-cooled spot, the seed crystal allowed the crystal growth to proceed on its faces by liquid-phase epitaxy, restricting the spontaneous nucleation, which significantly increases the size of the grown crystal. It should be

noted that the seeded growth remained the dominant process until the late stage of the growth, so that the grown crystal exhibits a pseudo-cubic morphology.

Compositional and structural analyses

In order to determine the composition and its homogeneity of the BS-PCN-PT crystal, the elementary analysis of five spots (areas of 100 × 75 μm^2 each) on a crystal plate (as shown in Fig. 3) was performed by means of energy dispersive X-ray spectroscopy (EDX). The inset graph in Fig. 3 shows the atomic percentages of the different elements detected in the specimen and their variations among the five spots. It can be seen that the compositions of different areas reveal almost the same contents of elements with little scattering. Table 1 summarizes the measured results and gives the calculated normalized compositions for five measured areas. The average composition of the as-grown crystals was determined to be 0.287BS-0.032PCN-0.681PT, with the percentage fluctuation for each element being less than ± 0.8. These results indicate that the composition of the BS-PCN-PT single crystals is homogenous when grown by the TSSG method, confirming that the TSSG method could indeed minimize the compositional segregation in the growth of multi-component solid solution single crystals.[20, 22, 25]

The phase and crystal structure of the BS-PCN-PT crystals were determined by high-resolution XRD on crushed crystals and the orientations of the natural facets of the crystals as examined by another high-resolution XRD instrument. The BS-PCN-PT crystals exhibit a typical perovskite structure with tetragonal symmetry, as evidenced by the splitting of the {00*l*} peaks in Fig. 4(a). From the XRD data, the lattice

parameters of the BS-PCN-PT single crystal were calculated to be a = 3.9785(5) Å and c = 4.1014(2) Å and the tetragonality, as defined by c/a, was found to be 1.0308(8), indicating a large tetragonal distortion. Figures 4(b) and (c) show the XRD patterns obtained on the natural facets of two representative platelets , which exhibit only three clear sets of {00*l*} peaks, confirming the $\{001\}_{cub}$ orientation of the crystals. According to the Bravais principle, crystal faces are most likely to come from the most densely populated and strongly bonded lattice planes due to their thermodynamic and mechanical stabilization. The primitive tetragonal perovskite structure has a pseudo-cubic lattice containing a lattice point at each of the eight corners.[26] Accordingly, the {100} plane has the highest density of lattice points, which results in the dominant {100}-growth process of the BS-PCN-PT crystals. In addition, Crystals #1 and #2 show different characteristics in their XRD patterns: Crystal #2 exhibits clearly split {00*l*} peaks, while Crystal #1 shows singlet for each {00*l*} peak, which might indicate the existence of a single ferroelastic domain state in Crystal #1. The inset in Fig. 4 shows various $(001)_{cub}$ oriented crystal platelets cut from the as-grown BS-PCN-PT crystal.

Domain structure

The optical domain structures of the BS-PCN-PT crystal were investigated by PLM. Figure 5 shows the images of two $(001)_{cub}$-oriented BS-PCN-PT crystals (#1 and #2) observed by PLM at room temperature. The optical observations were performed with the crossed polarizer (P) and analyzer (A) parallel, and at 45°, to the $<100>_{cub}$ direction. Figure 5(a-b) exhibits the extinction behavior of Crystal #1 ($1.3\times1\times0.85$ mm^3) which shows single {00*l*} peak on the XRD pattern (Fig. 4(b)). When observed along the [001]

direction, Crystal #1 is in extinction with crossed polarizers parallel (a), and at 45° (b), to the $<100>_{cub}$ direction (in fact, at any angle between the crossed polarizers). For Crystal #2, extinction occurs with the crossed polarizers at an angle of 0° or 90° to the $<100>_{cub}$ direction (Fig. 5(c)), while birefringent domain patterns were observed when the crossed polarizers were rotated by 45° to the $<100>_{cub}$ direction. The orientations of the optical indicatrix sections of different domains were identified with the help of a compensator, as indicated by the white circles or ellipses in Fig. 5(d). The extinction behaviors of Crystal #1 and #2 are both consistent with the optical characteristics of a tetragonal symmetry.[27] For the crystals of tetragonal phase, six possible spontaneous polarization directions exist parallel to the optical axes of the indicatrix. Therefore, when observed along the $<001>_{cub}$ direction, a $\{001\}_{cub}$ platelet exhibits domains with extinction angles at 0° or 90° in the tetragonal (T) phase, which is fully consistent with the extinction behaviors of Crystals #1 and #2.

The extinction behaviors of Crystal #1 were further investigated by PLM on the (001) and (100) faces, i. e. along the [001] and [100] crystallographic directions. The crystal was turned into a rectangular parallelepiped shape for PLM measurement by polishing based on the naturally grown {100} facets as reference. Figures 6(a) and (b) show the optical image of Crystal #1 and the schematic of its orientation. The PLM images are shown in Fig. 6 (c-h). When observed on the the (001) face with the light path parallel to the [001] direction, extinction occurs with crossed polarizers both parallel (Fig. 6(e)), and at 45° (Fig. 6(g)), to the $<100>_{cub}$ direction. However, when observed on the (100) face with the light propagating along the [100] direction, the extinction is observed when the crossed polarizers are at an angle of 0° or 90° to the $<100>_{cub}$ direction, but

no extinction appears at 45°, as shown in Fig. 6(f) and (h), respectively. This rules out the possibility of overlapping *a* domain layers, which should result in different extinction behaviors arising from those layers when the crossed polarizers are at 45°. Instead, the crystal appears to be homogenously anisotropic (birefringent) on the (100) as shown in Fig. 6(h), which proves the existence of a single *c* domain. The PLM results reveal the existence of a single ferroelastic domain state in Crystal #1 and a multi-domain state in Crystal #2, which supports the XRD results.

To understand the polarization behavior in Crystal #1, PFM measurements were carried out to further probe ferroelectric/polar domain structure, and the results are shown in Figure 7 in terms of topographic, amplitude and phase images. The out-of-plane (OOP) and in-plane (IP) amplitude and phase images are shown in Fig. 7(c-f). No obvious ferroelectric domain walls can be observed on the OOP phase images, indicating a homogenous distribution of polarization with a preferred orientation. Therefore, the crystal consists of a ferroelastic and ferroelectric single domain state. Figure 7(b) shows the switching of polarization by application of dc bias voltages, as revealed by OOP phase image. The outer square ($12 \times 12\ \mu m^2$) was first poled by a +30 V bias, and then the inner square ($4 \times 4\ \mu m^2$) was poled by a −30 V bias. Since a positive dc bias on the PFM tip switches the polarization downward and a negative dc bias upward, the phase of the as-grown crystal exhibits the same orientation as the positive bias, indicating a downward self-polarization.

In general, the crystals are prone to develop into multiple-domain states in order to lower the mechanical and electrostatic energy. It is known that, in the ferroelastic/ferroelectric tetragonal crystals of perovskite structure, two common types of domain walls are normally present: the 180° and 90° domain walls.[28] The unusual

formation of the single ferroelastic domain state in Crystal #1 implies that anisotropic mechanical stress might develop during the growth and the ferroelastic/ferroelectric phase transition, "poling" the crystal into a preferred orientation state with single ferroelastic domain state. More detailed study is needed to unveil the mechanism for the single-domain formation.

Ferroelectric, piezoelectric and dielectric properties

The polarization-electric field (*P*-*E*) hysteresis loops of the $(001)_{cub}$ BS-PCN-PT single crystals were displayed at room temperature at various field strengths, as shown in Figure 8. When a relatively low electric field (~20 kV/cm) is applied, the polarization in Crystal #1 partially switched and tend to switch back to its original state. Such switching behavior is similar to that of the pre-poled $BaTiO_3$ ceramics.[29] The saturation of polarization achieved at an electric field of 50 kV/cm at room temperature, as shown in Fig. 8. It should be noted that for both Crystals #1 and #2, clearly asymmetrical *P*-*E* loops are found at different fields. Both the negative E_c^- and positive E_c^+ shift to right with respect to the horizontal axis to a certain degree. Such shift could be attributed to the existence of an equivalent internal bias field defined as $E_{int} = (E_c^+ + E_c^-)/2$, which is commonly encountered in poled hard ferroelectrics.[30]

A large remanent polarization (P_r) of 24.8 μC/cm^2 is found in Crystal #1, and the remnant polarization reaches P_r = 19.2 μC/cm^2 for Crystal #2. The positive coercive electric fields (E_c^+) in the BS-PCN-PT crystals are found to be around 38 kV/cm for both Crystals #1 and #2, while the negative coercive electric fields (E_c^-) are smaller than the positive ones: 25.8 kV/cm for Crystal #1 and 31.3 kV/cm for #2. Moreover,

the average coercive field in Crystal #1 is calculated to be about 31.9 kV/cm and it is slightly higher (34.7 kV/cm) in Crystal #2. The higher remanent polarization and lower coercive field in Crystal #1 could be attributed to the different domain states from Crystal #2. The single ferroelastic domain state in Crystal #1 suggests that it would require no additional energy for ferroelastic domain and domain wall motions during the 180° ferroelectric domain switch, making the ferroelectric polarization switching easier, and thereby, leading to a lower E_c and a higher P_r. It should be noted that the E_c of the BS-PCN-PT single crystals is larger than that of the BS-PT system (~ 20 kV/cm)[8] and also much higher than that of relaxor-based PZN-PT and PMN-PT crystals (less than 5 kV/cm),[2-4] indicating a stable poled state which is suitable for potential applications that operate at high fields.

The piezoelectric coefficients d_{33} of the BS-PCN-PT crystals were measured before and after poling using a quasi-static d_{33} meter. The unpoled d_{33} value of Crystal #1 is 111 pC/N which is believed to arise from the self-polarization existing in the as-grown crystal, as evidenced by the PFM measurements. Interestingly, poling under 67.5 kV/cm for 15 min. does not increase the d_{33} value, which also confirms the self-polarization state in the as-grown crystals. Note that the d_{33} value of the BS-PCN-PT crystal is smaller than those of the PMN-PT or PZN-PT crystals of MPB compositions[2-4], which is mainly due to its tetragonal symmetry, but it is larger than the d_{33} value of tetragonal PT crystal (~ 50 pC/N)[29]. Further studies are underway to improve the piezoelectricity by exploring the BS-PCN-PT crystals of MPB compositions and optimizing the poling conditions.

Figure 9 shows the variations of the dielectric constant and loss tangent as a function

of temperature for Crystals #1 and #2. Both samples exhibit a sharp peak in the temperature dependence of dielectric constant, corresponding to the Curie temperature T_C of the phase transition from the ferroelectric to paraelectric phase upon heating. The value of T_C is found to be the same (423 ^{o}C) for both crystals, demonstrating that the phase transition temperature is independent of the domain states. This T_C value is higher than the conventional PZT-based materials and much higher than the PMN-PT and PZN-PT crystals, and it can be attributed to the large tetragonal distortion as evidenced by the structural analysis. It can be clearly seen from the inset image that the dielectric constant value of the single-domain Crystal #1 at temperature ≤ 200 ^{o}C is lower than that of Crystal #2. This phenomenon could be explained by the anisotropic character of the dielectric constant ε'. For instance, the anisotropic values of ε' measured in *a*-domain and *c*-domain $BaTiO_3$ crystals at room temperature[31] show $\varepsilon'_a > \varepsilon'_c$. Similarly, the multiple domain state including both *a* domain and *c* domain in Crystal #2 would give a higher dielectric constant than Crystal #1 with single *c*-domain. For both Crystals #1 and #2, the curves of dielectric loss stayed flat below 300 ^{o}C, indicating a good thermal stability. The room-temperature dielectric loss of the BS-PCN-PT crystal is about 0.02, and it remains low (< 0.15) even when the temperature reaches 500 ^{o}C, showing good dielectric properties.

Single domain ferroelastic/ferroelectric crystals play an important role in both fundamental research and technological applications.[32] From the scientific viewpoint, the intrinsic crystal physical properties that are anisotropic[33, 34], such as dielectric, piezoelectric, electromechanical and pyroelectric coefficient, etc., can only be obtained

on single domain crystals. As for the applications, single domain crystals are believed to have high thickness shear piezoelectric and pyroelectric properties.[35, 36] In addition, the high transmittance makes them ideal materials for optical and electrooptical applications without light scaterring caused by domain walls.[37] Moreover, polydomain crystals are prone to cracking during poling due to the large strain variation induced by ferroelastic domain switching. From this aspect, single domain crystals with self-polarization, like the BS-PCN-60PT crystals, exhibit another advantage: no need to be poled into a single domain state, which simplifies the preparation process and eleminates the risk of craking, leading to more cost-effective and reliable applications.

Conclusions

Single crystals of ternary solid solution $BiScO_3$-$Pb(Cd_{1/3}Nb_{2/3})O_3$-$PbTiO_3$ (BS-PCN-PT) have been successfully grown by top-seeded solution growth (TSSG) method. The grown crystals exhibit high compositional homogeneity and good quality, which proves that the TSSG method is an efficient technique to mitigate phase segregation in the growth of multi-component solid solution systems and it promotes the (001) growth, leading to a pseudo-cubic morphology. The crystal structure and domain structure of the grown crystals studied by high-resolution X-ray diffraction and Polarized Light Microscopy reveal a tetragonal symmetry with a large tetragonality. The BS-PCN-PT crystals are found to be ferroelectric with a Curie temperature T_C of 423 ^oC, which is much higher than the relaxor-based PMN-PT crystals. Most (001) platelets cut from the as-grown crystal exhibit a single ferroelastic domain state, and possess a high average

coercive field ($E_c \approx 30$ kV/cm) and a large remanent polarization (25 μC/cm^2). The ferroelectric domains of single-domain crystals were investigated by Piezoresponse Force Microscopy showing a self-polarization, which contributes to an unpoled piezoelectric constant d_{33} (111 pC/N). The high T_c, large coercive electric field, and high remanent polarization of the BS-PCN-PT crystals and unique single-domain sate make this material a promising candidate for both fundamental research applications and technological applications in a wide temperature range and at high power.

Conflicts of Interest

There are no conflicts to declare.

Acknowledgements

The powder XRD measurements were performed at University of Warwick, Coventry, UK, with the help of Dr. David Walker. The EDX work was carried out at International Center for Dielectric Research (ICDR), Xi'an Jiaotong University, Xi'an, China, with the help of Dr. Yijun Zhang. This work was supported by the National Natural Science Foundation of China (NSFC, Grants No. 61604123, 51602243 and 51902244), ‘‘the Fundamental Research Funds for the Central Universities’’ of China, the China Postdoctoral Science Foundation (Grant No. 2018M643632), the Natural Science Foundation of Shaanxi Province (Grant No. 2019JQ-389). The work at SFU was supported by the U. S. Office of Naval Research (ONR, Grant No. N0001416-1-3106) and the Natural Sciences and Engineering Research Council of Canada (NSERC, Grant No. 203773). Z. Luo would like to thank the China Scholarship Council (CSC) for supporting her visit to University of Warwick.

References

1. Z.-G. Ye, *MRS Bulletin*, 2009, **34**, 277-283.
2. S. Zhang, J. Luo, W. Hackenberger, N. P. Sherlock, R. J. Meyer Jr. and T. R. Shrout, *Journal of Applied Physics*, 2009, **105**, 104506.
3. E. Sun and W. Cao, *Progress in Materials Science*, 2014, **65**, 124-210.
4. S. Zhang, F. Li, X. Jiang, J. Kim, J. Luo and X. Geng, *Progress in Materials Science*, 2015, **68**, 1-66.
5. R. E. Eitel, C. A. Randall, T. R. Shrout, P. W. Rehrig, W. Hackenberger and S.-E. Park, *Japanese Journal of Applied Physics*, 2001, **40**, 5999-6002.
6. R. E. Eitel, C. A. Randall, T. R. Shrout and S.-E. Park, *Japanese Journal of Applied Physics*, 2002, **41**, 2099-2104.
7. S. Zhang, C. A. Randall and T. R. Shrout, *Applied Physics Letters*, 2003, **83**, 3150-3152.
8. S. Zhang, C. A. Randall and T. R. Shrout, *Journal of Applied Physics*, 2004, **95**, 4291-4295.
9. S. Zhang, C. A. Randall and T. R. Shrout, *Japanese Journal of Applied Physics*, 2004, **43**, 6199-6203.
10. M. Algueró, H. Amorín, T. Hungría, J. Galy and A. Castro, *Applied Physics Letters*, 2009, **94**, 012902.
11. J. Chen, H. Shi, G. Liu, J. Cheng and S. Dong, *Journal of Alloys and Compounds*, 2012, **537**, 280-285.
12. A. G. Segalla, S. S. Nersesov, G. M. Kaleva and E. D. Politova, *Inorganic Materials*, 2014, **50**, 606-611.
13. L. Kong, G. Liu, S. Zhang and W. Yang, *Applied Physics Letters*, 2015, **106**, 232901.

14. P. Long, G. Zhang and Z. Yi, *Materials Research Bulletin*, 2015, **66**, 213-218.

15. I. Sterianou, D. C. Sinclair, I. M. Reaney, T. P. Comyn and A. J. Bell, *Journal of Applied Physics*, 2009, **106**, 084107.

16. Z. Hu, J. Chen, M. Li, X. Li, G. Liu and S. Dong, *Journal of Applied Physics*, 2011, **110**, 064102.

17. E. D. Politova, G. M. Kaleva, A. V. Mosunov and A. H. Segalla, *Physica Scripta*, 2014, **89**, 044007.

18. T.-L. Zhao, J. Chen, C.-M. Wang, Y. Yu and S. Dong, *Journal of Applied Physics*, 2013, **114**, 027014.

19. Z. Luo, N. Zhang, Z. Liu, J. Zhuang, J. Zhao, W. Ren and Z.-G. Ye, *Journal of Materials Chemistry C*, 2018, **6**, 9216-9223.

20. X. Long and Z.-G. Ye, *Acta Materialia*, 2007, **55**, 6507-6512.

21. Q. Lu, X. Long and Y. Hu, *CrystEngComm*, 2010, **12**, 4317-4320.

22. W. Chen and Z.-G. Ye, *Journal of Crystal Growth*, 2001, **233**, 503-511.

23. C. He, X. Li, Z. Wang, Y. Liu, D. Shen, T. Li and X. Long, *CrystEngComm*, 2012, **14**, 4513-4519.

24. X. Li, Z. Wang, Y. Liu, C. He and X. Long, *CrystEngComm*, 2014, **16**, 7552-7557.

25. B. Wang, Y. Xie, J. Zhuang, X. Wu, W. Ren and Z.-G. Ye, *Journal of Applied Physics*, 2014, **115**, 084104.

26. M. Tachibana, *Beginner's Guide to Flux Crystal Growth*, Springer, Japan, 2017.

27. Z.-G. Ye and M. Dong, *Journal of Applied Physics*, 2000, **87**, 2312-2319.

28. P. R. Potnis, N.-T. Tsou and J. E. Huber, *Materials*, 2011, **4**, 417-447.

29. B. Jaffe, W. R. Cook and H. Jaffe, *Piezoelectric Ceramics*, Academic Press, London, 1971.

30. L. Jin, F. Li and S. Zhang, *Journal of the American Ceramic Society*, 2014, **97**, 1-27.

31. S. H. Wemple, M. Didomenico and I. Camlibel, *Journal of Physics and Chemistry of Solids*, 1968, **29**, 1797-1803.

32. F. Li, L. Wang, L. Jin, Z. Xu and S. Zhang, *CrystEngComm*, 2014, **16**, 2892-2897.

33. N. J. F., *Physical properties of crystals: their representation by tensors and matrices*, Oxford university press, 1985.

34. R. E. Newnham, *Properties of Materials: Anisotropy, Symmetry, Structure* Oxford University, New York, 2005.

35. F. Li, S. Zhang, Z. Xu, X. Wei and T. R. Shrout, *Advanced Functional Materials*, 2011, **21**, 2118-2128.

36. S. Zhang, F. Li, J. Luo, R. Sahul and T. R. Shrout, *IEEE Transactions on Ultrasonics, Ferroelectrics, and Frequency Control*, 2013, **60**, 1572-1580.

37. C. He, Z. Wang, X. Li, X. Yang, X. Long and Z.-G. Ye, *Acta Materialia*, 2017, **125**, 498-505.

Table 1. EDX elementary analysis results and calculated composition for a BS-PCN-PT crystal.

Measured Spot	Pb (at%)	Ti (at%)	Bi (at%)	Sc (at%)	O (at%)	Nb (at%)	Cd (at%)	Normalized Composition
1	11.30	11.29	4.34	5.52	66.6	0.92	0.01	0.293BS-0.036PCN-0.671PT
2	11.65	12.14	4.49	5.77	65.13	0.81	0.01	0.292BS-0.031PCN-0.677PT
3	11.96	12.52	4.53	5.54	64.66	0.78	0.01	0.283BS-0.029PCN-0.688PT
4	11.30	10.56	3.92	5.20	68.19	0.80	0.03	0.285BS-0.033PCN-0.682PT
5	11.33	11.11	4.13	5.05	67.61	0.75	0.02	0.281BS-0.031PCN-0.688PT
Average	11.51	11.52	4.28	5.42	66.44	0.81	0.02	0.287BS-0.032PCN-0.681PT

Table of Content

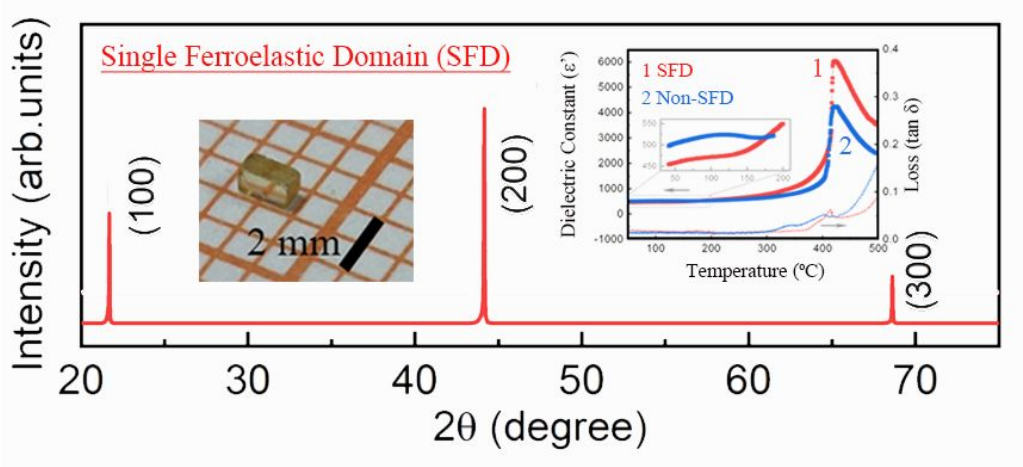

$BiScO_3$-$Pb(Cd_{1/3}Nb_{2/3})O_3$-$PbTiO_3$ single crystals with high quality have been successfully grown by top-seeded solution growth method and the single ferroelastic domain structures and ferroelectric behaviors haven also been reviewed.